ACCEPTED VERSION

Christopher N. Coleman, Patrick C. Tapping, Michael T. Huxley, Tak W. Kee, David M. Huang, Christian J. Doonan and Christopher J. Sumby

Structural modulation of the photophysical and electronic properties of pyrene-based 3D metal-organic frameworks derived from s-block metals

CrystEngComm, 2021; 23(1):82-90

Published at: http://dx.doi.org/10.1039/d0ce01505a

ARTICLE

Structural modulation of the photophysical and electronic properties of pyrene-based 3D metal–organic frameworks derived from s-block metals

Received 00th January 20xx,
Accepted 00th January 20xx

DOI: 10.1039/x0xx00000x

Christopher N. Coleman, Patrick C. Tapping, Michael T. Huxley, Tak W. Kee, David M. Huang*, Christian J. Doonan* and Christopher J. Sumby*

Materials in which charge delocalization and migration can be tuned are critical for electronic applications. Crystalline framework materials containing π-rich polycyclic aromatic moieties, such as pyrene, can provide a pathway for fast anisotropic charge transport. The extent of interchromophore interaction for structurally distinct assemblies of the π-conjugated aromatic ligand 4,4',4'',4'''-(1,3,6,8-pyrenetetrayl) tetrabenzoic acid (H_4TBAPy) was studied within two novel metal–organic frameworks (MOFs), Na(TBAPy)(DMF) and K(TBAPy)(DMF), via steady-state and time-resolved spectroscopic techniques. Single-crystal X-ray diffraction was used to determine the structures of K(TBAPy)(DMF) and Na(TBAPy)(DMF), which both form 3D MOFs comprising 1D rod-like SBUs surrounded by columnar stacks of TBAPy that are aligned in an eclipsed or x-shaped (staggered) geometry, respectively. Spectroscopic and computational results indicate significant chromophore interactions and potentially fast charge transport. Furthermore, distinct transient emission decay profiles are observed and are attributed to significant differences in the stacking orientation of the organic ligands in the two MOFs. Lastly, the study identifies design principles that may be exploited in the rational construction of s-block based MOFs for microelectronic and sensing applications.

Introduction

Metal–organic frameworks (MOFs) are a class of porous materials that are synthesized via a "building-block" approach from organic links and metal-based nodes.[1] They have been investigated for their potential applications in catalysis,[2] gas storage/separation,[3] biotechnology[4] and sensing.[5] However, in recent years, there has been a growing interest in the synthesis of electrically active MOFs.[6] One strategy that has been employed in the exploration of charge transport in both MOF, and related COF (covalent-organic framework) materials,[7] is to construct networks that possess π-rich organic components.[8] A design imperative of this approach is to position the organic linkers close enough together within the framework to allow for through-space charge transport.[9] However, this strategy represents a significant challenge for MOFs synthesized from carboxylate-functionalized linkers as they typically react with transition metal salts to form discrete inorganic nodes that engender 3D net topologies[10] in which the organic units are separated on length scales that preclude orbital overlap. An instructive example is the Zr-based MOF NU-1000, which is constructed from π-rich 4,4',4'',4'''-(1,3,6,8-pyrenetetrayl) tetrabenzoic acid (TBAPy) linkers that are separated by a minimum of 10.94 Å (centroid to centroid) due to the eight-coordinate Zr_6O_8 secondary building units (SBUs).[11] To overcome the geometrical constraints imposed by 0D nodes, 1D rod-like SBUs can be employed to facilitate close contact of the organic moieties. Although there are examples of infinite rod SBUs composed of transition metals (e.g. MIL-53[12] and MOF-74(M)[13]), we sought to synthesize TBAPy-based MOFs from s-block metals which are known to form 1D SBUs. The alkali metals sodium and potassium are particularly attractive precursor elements due to their availability, low cost and ecological compatibility.[14] Further, the network topologies of alkali metal MOFs are typically dominated by densely packed metal-O_n [n = 6–10] polyhedra, forming chains or layers, interconnected by organic linkers.[15] Nevertheless, the non-directional, ionic nature of s-block carboxylate bonds renders rational design of s-block MOFs a challenging task. The net-topologies of the s-block MOFs are heavily influenced by the shape and steric bulk of the ligands, π orbital interactions, as well as solvent polarity.[16] Thus, we surmised that an organic linker that has a strong preference to form π-stacked structures[17] may drive the formation of a network architecture with closely spaced or "stacked" TBAPy moieties. This hypothesis is supported by recent work showing that TBAPy is

Department of Chemistry and Centre for Advanced Nanomaterials, The University of Adelaide, Adelaide, South Australia 5005, Australia.
*email: christian.doonan@adelaide.edu.au, christopher.sumby@adelaide.edu.au; david.huang@adelaide.edu.au

Electronic Supplementary Information (ESI) available: additional experimental details for MOF synthesis and characterisation; fits for time resolved fluorescence data, additional crystallographic details, information of the fabrication of the LED device and further details of the calculations. See DOI: 10.1039/x0xx00000x

capable of forming a robust hydrogen-bonded organic framework (PFC-1)[18] that displays permanent porosity with a surface area of 2122 m^2g^{-1}, and exceptional chemical stability. It is noteworthy that computational analysis on PFC-1 clearly indicates significant pyrene–pyrene π orbital interactions that are responsible for the exceptional stability of this material.

Previously reported MOFs based on TBAPy (NU-1000, NU-901, ROD-7)[19,20,21] have been studied for their solid-state photophysical properties with a focus on interchromophoric interaction.[22] However, in these examples the chromophore spacing is larger than optimal (<4 Å), with the closest being an 8.76 Å centroid to centroid distance in the case of ROD-7. Thus, despite the intrinsic photoactivity of TBAPy, these MOFs are insulators and provide limited capacity for exciton delocalization or charge transport. In this study we report the synthesis of two new 3D MOFs based on TBAPy organic linkers and the s-block metal ions Na^+ and K^+, Na(TBAPy)(DMF) and K(TBAPy)(DMF), respectively. Structure determination, by single crystal X-ray diffraction (SCXRD), reveals that in these materials the pyrene moieties are positioned <4 Å apart with distinct eclipsed and x-shaped (staggered) arrangements, allowing for significant amplification of the pyrene–pyrene electronic coupling. Thus, given the close stacking arrangement observed for Na(TBAPy)(DMF) and K(TBAPy)(DMF) we examined their photoemission and charge-transport properties. Furthermore, Na(TBAPy)(DMF) and K(TBAPy)(DMF) offer the unique opportunity to compare how the relative alignment of the chromophores, “eclipsed” in K(TBAPy)(DMF) and a novel “x-shape” or staggered arrangement in Na(TBAPy)(DMF), influence the photophysical properties of the material. Indeed, time-resolved fluorescence spectroscopy, supported by computational analysis, suggests that energy transfer is sensitive to the orientation of the chromophores. In addition, to assess the viability of using these materials as semi-conductors, we fabricated a light-emitting diode (LED) that successfully integrates Na(TBAPy)(DMF) as a hole-transport layer.

Experimental

General details

All chemicals were obtained from commercial vendors (1,3,6,8 tetrabromopyrene, Sigma Aldrich, purity >97%; 4 ethoxycarbonylphenyl boronic acid, Boron Molecular, purity >97%) and used without further purification, unless otherwise stated. Dioxane was degassed with Ar prior to use. Tetraethyl 4,4′,4″,4‴-(pyrene-1,3,6,8-tetrayl) tetrabenzoate and the free carboxylic acid, H_4TBAPy, were synthesized using previously reported method[23] with some minor modification (see ESI Section 2). Powder X-ray diffraction data were collected on a Bruker Advance D8 diffractometer equipped with a capillary stage using Cu K_α radiation (λ = 1.5418 Å). NMR spectra were recorded on a Varian 500 MHz spectrometer operating at 23 °C and equipped with a 5 mm probe.

Single crystal X-ray diffraction (SCXRD)

Diffraction data were collected for single crystals mounted on nylon loops in Paratone-N at 100 K on the MX1 beamline of the Australian Synchrotron using the BluIce software interface,[24] λ = 0.71073 Å. N_{tot} reflections were merged to N_{unique} (R_{int} quoted) after a multi-scan absorption correction (proprietary software) and used in the full matrix least squares refinements on F^2, N_o with $F > 4\sigma(F)$ being considered 'observed'. The structure was solved using SHELXT[25] and refined using SHELXL[26], interfaced through the programs X-Seed[27] and Olex.[28] Unless otherwise stated, anisotropic displacement parameter forms were refined for the non-hydrogen atoms; hydrogen atoms were treated with a riding model [weights: $(\sigma^2(F_o)^2 + (aP)^2 + (bP))^{-1}$; $P = (F_o^2 + 2F_c^2)/3$]. Neutral atom complex scattering factors were used. Additional refinement details, crystallographic data and refinement parameters are found in the ESI (Section 4, Table S2).

Spectroscopy

Diffuse reflectance spectra were measured on solid samples using a Varian Cary 5000 spectrophotometer fitted with a Praying Mantis Diffuse Reflectance Accessory. Steady-state fluorescence measurements on solid samples were conducted on a Perkin Elmer LS 55 Spectrometer (slit widths: ex 2.5, em. 2.5 nm). Time-resolved fluorescence data were obtained using time-correlated single photon counting (TCSPC) on a Halcyone spectrometer sourced from Ultrafast Systems. Solid MOF samples were mounted inside 0.8 mm glass capillaries and measured in reflection mode. The 400 nm excitation light was generated by frequency doubling a portion of the output of a Ti-sapphire laser (Tsunami, Spectra Physics), with a pulse duration of ~100 fs. The repetition rate of the laser pulses was reduced from 80 MHz to 6.7 MHz with a Pockels cell pulse-picker. Multiexponential fits of the decay kinetics were performed using a function of the form $I(t) = \sum_n A_n \exp(-t/\tau_n)$ convoluted with a Gaussian instrument response function of 0.65 ns. Amplitudes are normalized so that $\sum_n |A_n| = 1$ (see ESI Section 3).

Quantum-chemical calculations

Density functional theory (DFT) calculations were performed with Q-Chem version 5.1.1.[29] Calculations of excited electronic states used time-dependent DFT (TD-DFT), while charge-transfer calculations used constrained density functional theory (CDFT)[30] and CDFT configuration interaction (CDFT-CI).[31,32] All geometries were optimized at the ωB97X-D/6-31G* level,[33] using DFT for ground states and TD-DFT for excited states. Single-point calculations were performed on optimized geometries at the ωB97X-D/6-31+G* level. All calculated electronic properties are at this level unless otherwise stated.

Carboxylate carbon and oxygen atom positions were constrained to their positions in the experimental crystal structure (carboxylate groups from the crystal structure were terminated by hydrogens to neutralize the charge). Ground-state geometry optimizations were initiated from the experimental crystal structure, while optimizations of excited states and charge-localized states were initiated from the optimized ground-state geometry.

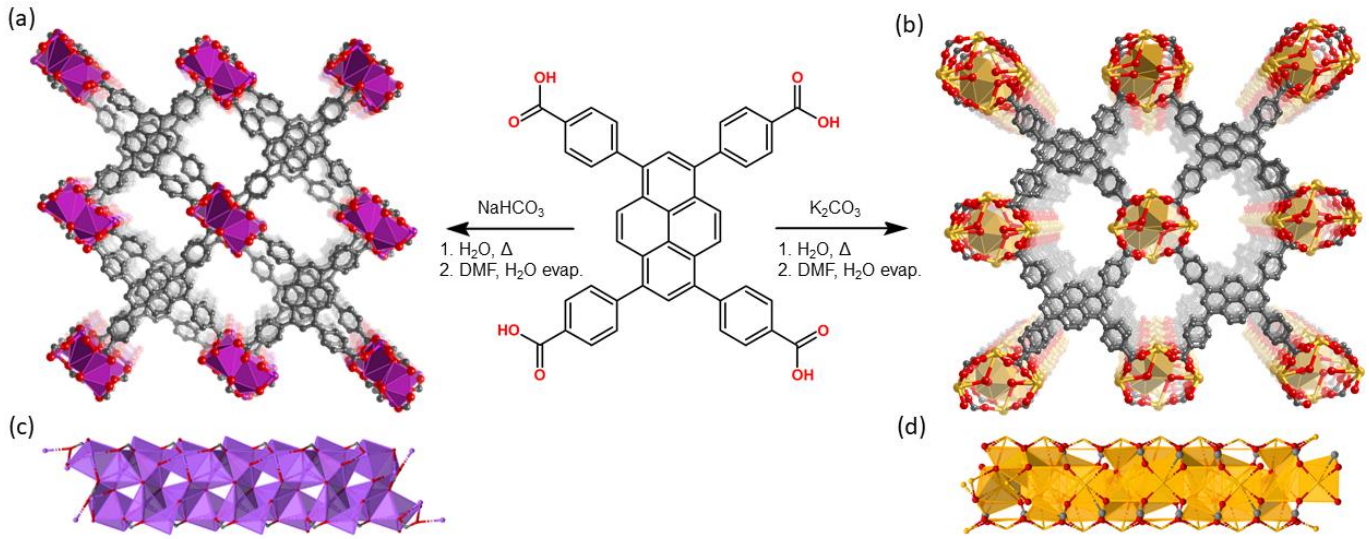

Fig. 1. Perspective views of the structures of the TBAPy-based MOFs obtained by single crystal X-ray diffraction (hydrogen and solvent molecules omitted for clarity). The extended structures of (a) Na(TBAPy)(DMF) and (b) K(TBAPy)(DMF), and their 1D SBUs (c) and (d), respectively, are provided. The materials used for all analyses were synthesised in the two-step procedures shown. Atoms are represented as: carbon (grey), oxygen (red), sodium (purple) and potassium (orange); hydrogen atoms and the non-coordinated atoms of solvate molecules are omitted.

MOF synthesis

Preparation of Na(TBAPy)(DMF). H_4TBAPy (50 mg, 73 µmol) and $NaHCO_3$ (25 mg, 0.29 mmol) were suspended in water (30 mL) and the solution was heated at reflux for 24 hours. The reaction mixture was allowed to cool, and the water was removed under vacuum. The yellow solid was then dissolved in a mixture of DMF (5 mL) and water (5 mL) which was allowed to slowly evaporate over several days resulting in the formation of needle-like yellow crystals of Na(TBAPy)(DMF), which were washed with DMF (see Fig. S10).

Crystals suitable for SCXRD were grown by slow vapor diffusion of acetone into a concentrated solution of Na(TBAPy)(DMF) in DMF/H_2O (1:1). The resulting yellow rod-shaped crystals (Na(TBAPy)(acetone) were suitable for SCXRD. These were then transferred to a solution of DMF and allowed to soak for several days in order to exchange the coordinated acetone for DMF and give Na(TBAPy)(DMF). IR (ν_{max}, cm^{-1}): 1675 (s, CO), 1603 (m, CO), 1374 (s, C=C), 1269 (s, CO).

Preparation of K(TBAPy)(DMF). H_4TBAPy (50 mg, 73 µmol) and K_2CO_3 (40 mg, 0.29 mmol) were dissolved in water (30 mL) and the solution was heated at reflux for 24 hours. The reaction mixture was allowed to cool, and the water was removed under vacuum. The yellow solid was then dissolved in a mixture of DMF (5 mL) and water (5 mL) and the solution was allowed to slowly evaporate over several days resulting in the formation of needle-like yellow crystals of K(TBAPy)(DMF) which were washed with DMF (see Fig. S10). Crystals suitable for SCXRD were grown by a solvothermal method. TBAPy (25 mg, 37 µmol) and K_2CO_3 (20mg, 0.14 mmol) were added to DMF (4 mL), water (2 mL) and conc. HCL (80 µL) in a 20 mL glass vial. The solution was heated at 100°C for 24 hours to give yellow rod-shaped crystals of K(TBAPy)(DMF). IR (ν_{max}, cm^{-1}): 3290 (br, C-H), 1685 (m, CO), 1608 (s, CO), 1401 (s, C=C).

Preparation of LED Device

An glass indium-tin oxide (ITO) glass substrate was coated with Na(TBAPy)(DMF) and a light emitting copolymer (PDOF and MEH-PPV). Details of the device fabrication are in the ESI (Fig. S11).

Results and discussion

MOF synthesis and structures

Na(TBAPy)(DMF) and K(TBAPy)(DMF) were synthesized by reacting an aqueous suspension of H_4TBAPy with sodium carbonate or potassium carbonate, respectively, under reflux for 24 hours to form the TBAPy salts (Fig. 1). Removal of water afforded pale-yellow powders that were recrystallized via slow evaporation from DMF/H_2O to yield pure crystalline material (see Figs. S2 and S10). Single crystals for an acetone-solvated form of the sodium MOF were obtained by vapor diffusion of acetone into a concentrated 1:1 DMF/H_2O solution of Na(TBAPy)(DMF), followed by solvent exchange with DMF to form the DMF solvate, Na(TBAPy)(DMF) (see Fig. S4 for a structural comparison); single crystals of K(TBAPy)(DMF) were obtained by a solvothermal method.

Na(TBAPy)(DMF) crystallizes in the monoclinic space group $P2_1/n$. The ligand occupies two distinct chemical environments, with an asymmetric unit consisting of two partial ligands (one complete TBAPy molecule), four sodium atoms and two coordinated DMF molecules; this gives the formula [Na_4(TBAPy)$(DMF)_2$]. The structure of Na(TBAPy)(DMF)

comprises a 1D SBU extending along the *b* axis (Fig. 1c), with the ligand acting as a four connecting centre. Within the linear SBU, the metal centres are present in trigonal prismatic and distorted octahedral coordination geometries. The coordination environment of the sodium SBU includes ionic bonding to oxygen atoms of carboxylate and solvent molecules, as well as bridging water molecules. The orientation by which the linkers stack is unique. As opposed to an eclipsed or "slip stacked" arrangement, the pyrene cores form an x-shape (see Figs. 1a and 4b) and the 4 benzoate groups on each ligand form two co-facial and two edge-to-face π-stacking interactions with neighbouring ligands. Furthermore, subtle structural changes can be induced for the Na-based material by exchanging the solvent and altering the crystallization methods. Powder X-ray diffraction (PXRD) (Fig. S3) shows two distinct forms of the sodium-based MOF can be obtained, namely Na(TBAPy)(DMF) and Na(TBAPy)(acetone). Sodium is prone to coordinate a variety of solvents, and well-defined solvent molecules appear as integral features of the molecular composition, with Na(TBAPy)(acetone) featuring coordinated acetone in place of DMF but also coordinated water which subtly modifies the diameter of the SBU (see Fig. S4) and the unit cell.

K(TBAPy)(DMF) crystallizes in monoclinic space group $P2_1/c$. The asymmetric unit consists of two ligand molecules, nine potassium atoms, coordinated solvent (DMF and water), and a 50% occupied carbonate anion: $[K_9(TBAPy)_2(H_2O)_{8.25}(DMF)_{3.25}(CO_3)_{0.5}]$. A salient feature of K(TBAPy)(DMF) is that, in contrast to Na(TBAPy)(DMF), the TPABY links are aligned in an eclipsed formation (Fig. 1b). This arrangement results in all carbon atoms in the stacked pyrene moieties separated by ca. 3.85 Å, with the ligands aligning in an extended H-aggregate configuration.[34,35] The larger unit cell in the potassium MOF is the result of disordered solvent molecules which alter the dihedral angles on adjacent TBAPy molecules (see Fig. S9). However, despite these crystallographic differences and in contrast to Na(TBAPy)(DMF), the linkers of K(TBAPy)(DMF) are stacked directly on top of each other with all ligands having almost identical chemical environments. This is an important consideration in the analysis of the spectral data. The SBU in K(TBAPy)(DMF) comprises 1D potassium oxide chains (Fig. 1d). The potassium ions co-ordinate with up to 7 oxygen atoms that include carboxylate groups, DMF and water molecules. PXRD data for a sample of K(TBAPy)(DMF) obtained by slow evaporation matches the structure determined by single crystal diffraction, thus confirming bulk purity (see Fig. 2).

Due to the 1D rod-like SBUs that feature in Na(TBAPy)(DMF) and K(TBAPy)(DMF), close-packing of the pyrene moieties is observed. This, in theory, has the potential to facilitate charge transfer through π-orbital overlap as well as trigger noticeable interchromophoric interactions. The close packing of linkers also appears to confer some stability to the MOFs. The result is that both structures are stable and retain their crystallinity for months after being removed from solvent, provided they are kept in an environment devoid of excess moisture.

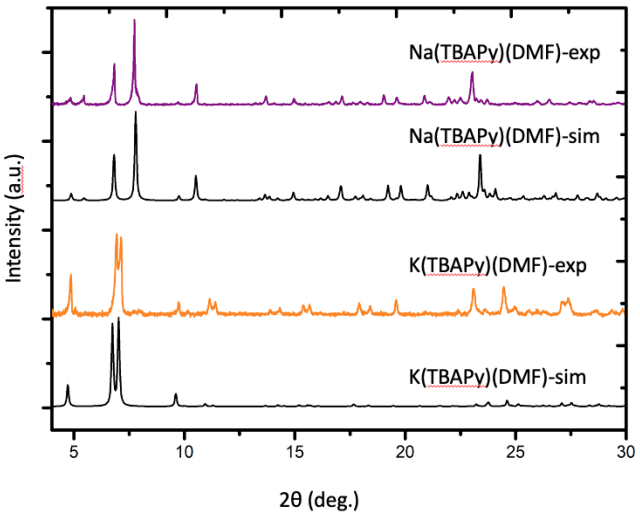

Fig. 2. Simulated (sim) and experimental (exp) PXRD patterns of Na(TBAPy)(DMF) and K(TBAPy)(DMF).

Photophysical properties

In terms of fluorescence quantum yield and excited state lifetime, pyrene ranks considerably higher than many well-known and commonly employed chromophores.[36] Additionally, its spectral signature is well known to be sensitive to its environment.[37] Pyrene-based MOFs have been investigated for their photophysical performance characteristics; however, Na(TBAPy)(DMF) and K(TBAPy)(DMF) provide an unprecedented opportunity to examine the effects of chromophore alignment in two close-stacked systems. Thus, to understand the nature of the chromophoric interactions we carried out steady-state and time-resolved spectroscopic studies on each MOF. We anticipated that the different stacking arrangements present in Na(TBAPy)(DMF) and K(TBAPy)(DMF) would manifest distinct emission decay profiles as a function of their topology. Previously reported spectral data for pyrene derivatives showed solvent-dependent emission peaks for the same materials.[38,39,40] To avoid the effects of solvent polarity on the excited state energy we conducted spectroscopic studies on dried material.

The high chromophore density in Na(TBAPy)(DMF) and K(TBAPy)(DMF) should result in effective photon absorption. The calculated molar density of TBAPy in each framework was 1.62 mol dm^{-3} for Na(TBAPy)(DMF) and 1.40 mol dm^{-3} for K(TBAPy)(DMF). We note that both values are considerably higher than that of the zirconium-based MOF NU-1000 (0.41 mol dm^{-3}).[39] Close positioning of photoactive ligands typically leads to nonradiative pathways that can quench fluorescence.[41] However, despite the proximity of the pyrene groups in Na(TBAPy)(DMF) and K(TBAPy)(DMF), both MOFs are fluorescent in the solid state. The solid-state absorption profile features distinct peaks and troughs ranging from 225 to 450 nm (with a maximum ca. 405 nm). Despite the different relative orientations of the TBAPy ligands in the two MOFs, both show almost identical absorption profiles, as shown in Fig. 3a.

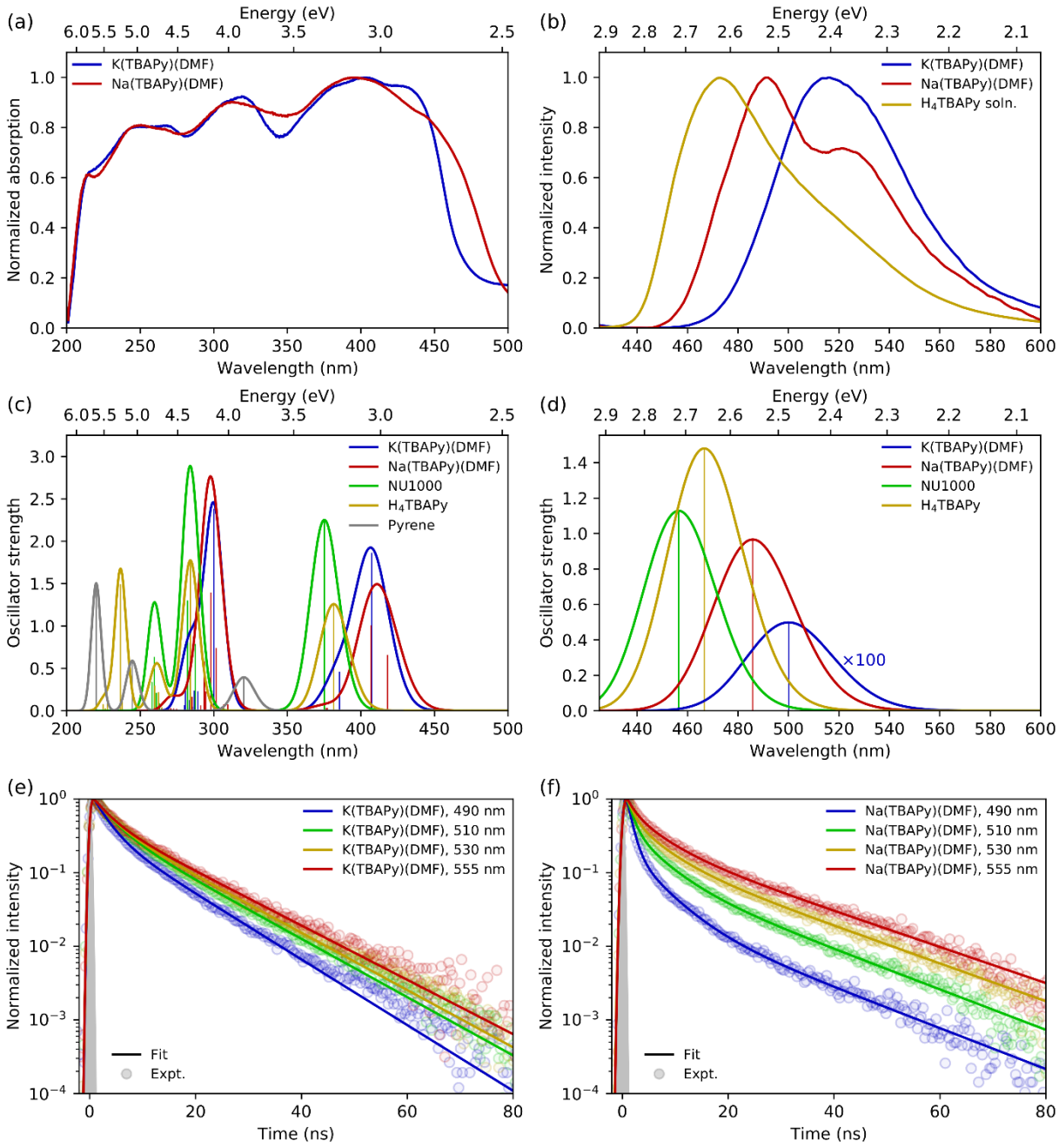

Fig. 3. (a) Solid-state absorption spectra (measured by diffuse reflectance) of K(TBAPy)(DMF) (blue) and Na(TBAPy)(DMF) (red). (b) Emission spectra for solid-state K(TBAPy)(DMF) (blue) and K(TBAPy)(DMF) (red) using 405 nm excitation, with the H_4TBAPy linker in DMF solution (yellow) for reference. Calculated (c) absorption and (d) emission spectra for the same species, with spectra for NU-1000 (green) and pyrene (grey) included for reference (computed spectra have been red-shifted by 0.4 eV and convoluted with a Gaussian of full width at half maximum (FWHM) of 0.2 eV in all cases). Time-resolved fluorescence kinetics at different detection wavelengths for (e) K(TBAPy)(DMF) and (f) Na(TBAPy)(DMF). Fits to a multiexponential decay model are shown with solid lines, with fitting parameters given in Table S1. The experimentally determined instrument response is indicated with the grey shaded region corresponding to a Gaussian function of 0.65 ns FWHM.

The solid-state emission spectra for K(TBAPy)(DMF) and Na(TBAPy)(DMF) are shown in Fig. 3b. The emission peak of K(TBAPy)(DMF) is centred at 515 nm and largely featureless but is significantly red shifted compared to that of the free H_4TBAPy linker in solution. In contrast, the Na(TBAPy)(DMF) emission band exhibits distinct spectral structure, with the main peak at 490 nm and shoulder around 530 nm. The shift of the emission peaks to lower energies relative to the free H_4TBAPy linker in solution is indicative of electronic coupling between the chromophore units resulting from close packing of the aromatic pyrene cores of the TBAPy linkers in the solid-state. This molecular architecture allows significant π–π interactions, and thus delocalization of the excitation. The spectral structure evident in the Na(TBAPy)(DMF) emission can be attributed to a vibronic progression. The shoulder is lower in energy than the main peak by approximately 1600 cm^{-1}, which can be assigned

to the aromatic C=C bond vibration in the pyrene cores. The absence of structure in the K(TBAPy)(DMF) emission can be attributed to the distinct alignments of the pyrene units observed in the two MOFs. The packing of the linkers in K(TBAPy)(DMF) resembles that of an ideal H-aggregate,[35,42] in which the eclipsed arrangement of the chromophore pairs suppresses the 0–0 vibronic transition, leaving the 0–1 peak to dominate the spectrum. The x-shaped stacking of the linkers in Na(TBAPy)(DMF) results in coupling that is intermediate between that of a J- and an H-aggregate, and thus the 0–0 and 0–1 vibronic peaks are both present. This aggregate behaviour can also account for the differences between the absorption spectra of the MOFs (Fig. 3a), which show that absorption in the Na(TBAPy)(DMF) extends further into the low-energy region, while the lowest energy 0–0 vibronic absorption peak is attenuated in K(TBAPy)(DMF).

Fluorescence decay kinetics were obtained for the two MOFs at several emission wavelengths, shown in Figs. 3e and 3f. The data were fit to a multiexponential decay model, with parameters given in Table S1. For K(TBAPy)(DMF), the kinetic profiles are almost identical at all detection wavelengths. The slightly faster decay at 490 nm is at the blue edge of the absorption peak and is indicative of spectral migration to lower energies due to excited-state structural relaxation or exciton migration. Na(TBAPy)(DMF), however, displays significantly different kinetics at each detection wavelength, with noticeably faster decays at shorter wavelengths, particularly at short times ($\lesssim$5–10 ns), which also indicates time-dependent spectral migration, but to a greater extent and at a faster rate than that observed in K(TBAPy)(DMF). The longer time ($\gtrsim$5–10 ns) decay, which occurs approximately uniformly across all wavelengths in both MOFs, can be attributed to relaxation to the ground state. The faster decays on both time scales in Na(TBAPy)(DMF) compared with K(TBAPy)(DMF) can again be attributed to the arrangement of the chromophores within the MOFs, as the H-aggregate[35] nature of K(TBAPy)(DMF) is expected to result in slower emission and reduced exciton migration by resonance energy transfer.

Although pyrene dimers stacked directly on top of each other have been observed and probed previously,[43] to the best of our knowledge the x-shaped or staggered configuration of pyrene present in Na(TBAPy)(DMF) (Fig. 4) has not been documented. To clarify how the configuration of ligands influences the electronic coupling and excited-state properties in the two s-block MOFs, we performed density functional theory (DFT) calculations on the two closest ligand pairs in each MOF, with which the carboxylate C and O atoms fixed at their positions in the experimental SCXRD structure to mimic the coordination constraints in the MOF. For comparison, analogous calculations were performed on the closest ligand pair in NU-1000 and similar calculations were performed on the TBAPy monomer and on pyrene without geometric constraints. Absorption and emission spectra were calculated using time-dependent DFT (TD-DFT) on the optimized geometry of the electronic ground state and first excited state, respectively. Details of the calculations are given in the ESI.

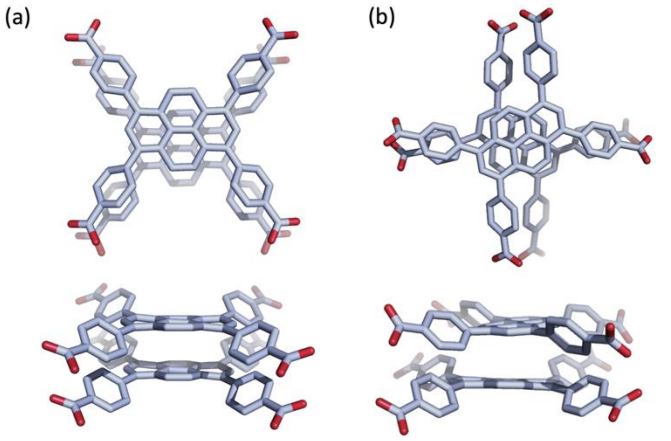

Fig. 4. Relative orientation of the TBAPy ligand in (a) K(TBAPy)(DMF), eclipsed, and (b) Na(TBAPy)(DMF), x-shaped. The TBAPy ligands are viewed along the crystallographic *b* axis (top) and *a* axis (below).

Consistent with experiment, the absorption spectra of the K(TBAPy)(DMF) and Na(TBAPy)(DMF) MOFs calculated by TD-DFT on the optimized ground-state geometries of the constrained ligand dimers have similar peak positions but are blue-shifted (by ~0.4–0.6 eV) compared with experiment, as shown in Fig. 3c. However, the lowest energy absorption transitions are shifted to lower energy compared with those the NU-1000 MOF and the TBAPy monomer (by ~0.2 eV in both cases), indicating substantially stronger electronic coupling between the ligands in K(TBAPy)(DMF) and Na(TBAPy)(DMF) compared with NU-1000. The discrepancy between the calculations and experiment can be partly attributed to using a dimer model in the calculations, which neglects coupling between multiple ligands in the MOF. Also calculated is the absorption spectrum of pyrene, which is significantly blue shifted compared with the TBAPy monomer, indicating significant electron delocalization between the pyrene and phenyl groups in H_4TBAPy.

The calculations show that the transition dipole moment (TDM) of the lowest energy transition of the TBAPy monomer is aligned in the plane along the long axis of the pyrene core, as shown in Fig. S13a. The orientation of the ligands in the Na(TBAPy)(DMF) MOF dimer at an angle to one another (105°) results in an excited-state electronic coupling that is intermediate between a H and a J-type interaction, producing two almost degenerate lowest energy absorption transitions (separated by ~0.08 eV) with significant TDMs that are almost orthogonal to one another, as shown in Fig. S13b. On the other hand, confirming our interpretation of the spectroscopic data, the parallel orientation of the monomers in the K(TBAPy)(DMF) MOF dimer yields an H-type interaction, with the lowest energy absorption transition having negligible oscillator strength and the most intense transition being the second lowest, which has a TDM aligned in the same direction as that of the TBAPy monomer (Fig. S13c).

Also consistent with the experiment, the emission of the Na(TBAPy)(DMF) MOF dimer is red-shifted by ~0.4 eV with respect to absorption due to structural relaxation of the excited

state (Fig. 3d), but the Stokes shift is about half that observed experimentally. This discrepancy is likely due to the strong geometric constraints placed on the carboxylate atom positions in the calculations, which neglect flexibility of the MOF. As shown in Fig. S12, the atoms in the Na(TBAPy)(DMF) MOF dimer hardly move between the ground and excited-state geometries. The Stokes shift calculated for the TBAPy monomer, for which no geometric constraints were applied, is significantly larger, at ~0.6 eV. This larger shift appears to be related to the larger change in the dihedral angle between the pyrene core and phenyl substituents in the excited state of the monomer compared with the MOF dimers, which leads to greater electron delocalization due to the more planar geometry. Calculations on the K(TBAPy)(DMF) MOF dimer indicate that the purely electronic $S_1 \rightarrow S_0$ transition does not occur, which is consistent with the presence of H-type coupling, with emission made possible by vibronic coupling that is neglected in our purely electronic calculations.

Unlike previous reports examining the topology-dependent emissive properties of MOFs containing the TBAPy ligand,[44,22] we were reluctant to classify the emission as resulting from excimer formation. Although our model overestimates how rigidly the ligands are held in position, we see no strong evidence to suggest that the experimentally observed steady-state or time-resolved emission are a result of significant geometric rearrangement of the ligands within the lattice that would be associated with excimer formation . The Stokes shift[45] and peak width of the steady-state emission of both s-block MOFs is much smaller than that associated with excimer formation in pyrene, and the emission is not substantially broadened compared with the isolated TBAPy ligand, as shown in Fig. 3b. In addition, the shortest decay times measured in the time-resolved emission are an order of magnitude longer than that of excimer formation in crystalline pyrene.[45] Furthermore, the calculated changes in the excited-state geometry compared with the ground-state geometry are much smaller than those calculated for pyrene excimers.[46,43]

Charge-transport properties

Although most MOFs are insulators with no capacity for exciton delocalization between ligands, intrinsic charge transport within a MOF is still an area of emerging interest.[47] A design challenge for electrically conductive MOFs is that charge transport decreases exponentially with increased intermolecular distance between frontier orbitals.[48] We have shown that the two s-block MOFs presented in this work possess a close packed arrangement of π-rich chromophores and thus may facilitate exciton delocalization and charge mobility. However, conductivity experiments on microcrystalline materials are notoriously unreliable and can differ by orders of magnitude.[49] For this reason we decided to use quantum-chemical calculations to estimate the effect of the relative position and orientation of the ligands on charge-transfer rates in the s-block MOFs and a related pyrene-based MOF. Charge-transfer parameters for hole transfer in the K(TBAPy)(DMF) and Na(TBAPy)(DMF) MOFs were calculated and compared with those for NU-1000. Constrained density functional theory (CDFT) was used to localize a +1 charge on one of the monomers in each MOF dimer and CDFT-CI was used to calculate the electronic coupling V_{da} and reorganization energy λ for the process of transferring this +1 charge from one monomer to the other. The hole transfer rate constant k_h was also calculated using Marcus theory[50] according to

$$k_h = \frac{2\pi}{\hbar}|V_{da}|^2\sqrt{\frac{1}{4\pi k_B T\lambda}}\exp\left[-\frac{(\Delta G^\circ+\lambda)^2}{4\lambda k_B T}\right] \quad (1)$$

where ΔG° is the free-energy change for the process (which is zero here because the hole donor and acceptor are the same), T is the temperature, k_B is the Boltzmann constant and $\hbar$ is the reduced Planck's constant. As shown in Table S3, although the reorganization energy for all three MOFs is similar, the electronic couplings in the K(TBAPy)(DMF) and Na(TBAPy)(DMF) MOFs are both an order-of-magnitude larger than that of NU-1000, as a result of the much closer spacing between the ligands in these MOFs (<4 Å). Consequently, the calculated hole-transfer rate constants for K(TBAPy)(DMF) and Na(TBAPy)(DMF) are two orders of magnitude larger than that of NU-1000, due to the quadratic dependence of the rate constant on the coupling (see Table 1). Furthermore, the different relative orientation of the ligands in the K(TBAPy)(DMF) and Na(TBAPy)(DMF) MOFs results in the electronic coupling and hole-transfer rate constant being respectively a factor of two and four larger for Na(TBAPy)(DMF) compared with K(TBAPy)(DMF). This result suggests that charge-transfer properties can be strongly modulated by ligand configuration in these closely related MOFs.

Table 1. Calculated electronic couplings, reorganization energies, and hole-transfer rate constants for MOF TBAPy dimers.

MOF	hole transfer rate constant k_h (s^{-1})	two closest ligands (centroid to centroid)
Na(TBAPy)(DMF)	5.7×10^{12}	3.93 Å
K(TBAPy)(DMF)	1.5×10^{12}	3.86 Å
NU-1000	3.3×10^{10}	10.94 Å

Given the encouraging results from quantum-chemical calculations, coupled with the well documented ability of pyrene moieties to facilitate hole transfer in several electronically active polymers and composites,[51] we examined the semiconducting properties of Na(TBAPy)(DMF) by using it to construct a light emitting diode (LED). LEDs generally consist of a conductive substrate, a hole transport layer, and a light-emitting layer.[52] Poly(3,4-ethylenedioxythiophene) polystyrene sulfonate (PEDOT:PSS) can be used as an effective hole transport layer[53] that can prevent the LED from shorting, and transports positive charge to the active light emitting polymer layer.[54] While the PEDOT:PSS layer does not itself emit any light, such hole transport layers have been found to dramatically improve the efficiency of polymer-based LEDs.[55] To this end, we substituted PEDOT:PSS for Na(TBAPy)(DMF) to yield a functioning LED which emitted at 580 nm with a voltage of 4.45 V (24 mA) (see Fig. S11). Control devices that consisted of just the conductive substrate and the light emitting layer, with no hole transport layer, failed to

function. Upon introduction of an electric current, these devices immediately began to heat and did not emit any light. The functioning device represents the first time a sodium-based MOF has been used as a semiconducting hole transport layer in a functioning LED.

Conclusion

We successfully synthesized two new, stable, non-interpenetrated s-block-based MOFs, Na(TBAPy)(DMF) and K(TBAPy)(DMF), containing a π-rich photoactive organic linker. As anticipated, the non-directional, ionic metal-ligand bonds yields MOFs possessing rod-like SBUs and close proximity of the pyrene moieties. Interestingly, the pyrene chromophores adopt different relative packing arrangements (eclipsed and x-shaped) that according to computational and spectral data give rise to significantly different electronic coupling. We note that this is the first time an x-shaped (staggered) alignment of pyrene cores has been examined in the solid-state. This work shows that there is broad scope for using s-block MOFs composed of π-rich chromophores for a variety of sensing and electronic applications. Furthermore, they are ideal candidates for fundamental studies on how the level of solvation, solvent polarity, ion exchange, guest molecules, chromophore packing and alignment, and photoinduced structural changes influence the electronic properties of a material.

Conflicts of interest

There are no conflicts to declare.

Acknowledgements

This research was undertaken with the assistance of resources and services from the National Computational Infrastructure (NCI), which is supported by the Australian Government, and from The University of Adelaide's Phoenix High Performance Computing service. This research was undertaken in part using the MX1 beamline at the Australian Synchrotron, part of ANSTO. The time-resolved fluorescence studies were performed at a laser spectroscopic facility supported by the Australian Research Council (ARC, LE0989747) and in-house single crystal X-ray diffraction undertaken on equipment provided under ARC grant LE0989336.

References

1 (a) O. M. Yaghi, M. O'Keeffe, N. W. Ockwig, H. K. Chae, M. Eddaoudi and J. Kim, *Nature*, 2003, **423**, 705–714; H. Furukawa, K. E. Cordova, M. O'Keeffe and O. M. Yaghi, *Science*, 2013, **341**, 1230444.

2 (a) V. Pascanu, G. González Miera, A. K. Inge and B. Martín-Matute, *J. Am. Chem. Soc.*, 2019, **141**, 7223–7234; (b) D. Yang and B. C. Gates, *ACS Catal.*, 2019, **9**, 1779–1798.

3 (a) Z. Kang, L. Fan and D. Sun, *J. Mater. Chem. A*, 2017, **5**, 10073–10091; (b) X. Zhao, Y. Wang, D.-S. Li, X. Bu and P. Feng, *Adv. Mater.* 2018**, 30**, 1705189.

4 (a) K. Liang, R. Ricco, C. M. Doherty, M. J. Styles, S. Bell, N. Kirby, S. Mudie, D. Haylock, A. J. Hill, C. J. Doonan and P. Falcaro, *Nat. Commun.*, 2015, **6**, 7240; (b) J. W. M. Osterrieth and D. Fairen-Jimenez, *Biotech. J.*, 2020**,** https://doi.org/10.1002/biot.202000005.

5 W. P. Lustig, S. Mukherjee, N. D. Rudd, A. V. Desai, J. Li and S. K. Ghosh, *Chem. Soc. Rev.*, 2017, **46**, 3242–3285.

6 L. Sun, M. G. Campbell and M. Dinca, *Angew. Chem. Int. Ed.*, 2016, **55**, 3566–3579.

7 H. Yang, S. Zhang, L. Han, Z. Zhang, Z. Xue, J. Gao, Y. Li, C. Huang, Y. Yi, H. Liu and Y. Li, *ACS Appl. Mater. Interfaces*, 2016, **8**, 5366–5375.

8 Y. Gao, H. Liu, S. Zhang, Q. Gu, Y. Shen, Y. Ge and B. Yang, *Phys. Chem. Chem. Phys.*, 2018, **20**, 12129–12137.

9 T. C. Narayan, T. Miyakai, S. Seki and M. Dincă, *J. Am. Chem. Soc.*, 2012, **134**, 12932–12935.

10 K. S. Lin, A. K. Adhikari, C. N. Ku, C. L. Chiang and H. Kuo, *Int. J. Hydrogen Energy*, 2012, **37**, 13865–13871.

11 T. Zhang, P. Wang, Z. Gao, Y. An, C. He and C. Duan, *RSC Adv.*, 2018, **8**, 32610–32620.

12 C. W. Ashling, D. N. Johnstone, R. N. Widmer, J. Hou, S. M. Collins, A. F. Sapnik, A. M. Bumstead, P. A. Midgley, P. A. Chater, D. A. Keen and T. D. Bennett, *J. Am. Chem. Soc.*, 2019, **141**, 15641–15648.

13 J. Wang, Y. Fan, H. W. Lee, C. Yi, C. Cheng, X. Zhao and M. Yang, *ACS Appl. Nano Mater.*, 2018, **1**, 3747–3753.

14 S. Krieck and M. Westerhausen, *Inorganics*, 2017, **5**, 8–11.

15 D. Banerjee and J. B. Parise, *Cryst. Growth Des.*, 2011, **11**, 4704–4720.

16 D. L. Reger, A. P. Leitner and M. D. Smith, *Cryst. Growth Des.*, 2016, **16**, 527–536.

17 C. G. Perkins, J. E. Warren, A. Fateeva, K. C. Stylianou, A. McLennan, K. Jelfs, D. Bradshaw and M. J. Rosseinsky, *Micropor. Mesopor. Mater.*, 2012, **157**, 24–32.

18 Q. Yin, P. Zhao, R.-J. Sa, G.-C. Chen, J. Lü, T.-F. Liu and R. Cao, *Angew. Chem. Int. Ed.*, 2018, **57**, 7691–7696.

19 T. Islamoglu, K. I. Otake, P. Li, C. T. Buru, A. W. Peters, I. Akpinar, S. J. Garibay and O. K. Farha, *CrystEngComm*, 2018, **20**, 5913–5918.

20 S. J. Garibay, I. Iordanov, T. Islamoglu, J. B. DeCoste and O. K. Farha, *CrystEngComm*, 2018, **20**, 7066–7070.

21 R. J. Li, M. Li, X. P. Zhou, D. Li and M. O'Keeffe, *Chem. Commun.*, 2014, **50**, 4047–4049.

22 J. Yu, J. Park, A. Van Wyk, G. Rumbles and P. Deria, *J. Am. Chem. Soc.*, 2018, **140**, 10488–10496.

23 T. C. Wang, N. A. Vermeulen, I. S. Kim, A. B. F. Martinson, J. F. Stoddart, J. T. Hupp and O. K. Farha, *Nat. Protoc.*, 2016, **11**, 149–162.

24 T. M. McPhillips, S. E. McPhillips, H. J. Chiu, A. E. Cohen, A. M. Deacon, P. J. Ellis, E. Garman, A. Gonzalez, N. K. Sauter, R. P. Phizackerley, S. M. Soltis and P. Kuhn, *J. Synchrotron Radiat.*, 2002, **9**, 401–406.

25 G. M. Sheldrick, *Acta Crystallogr. Sect. A Found. Crystallogr.*, 2015, **71**, 3–8.

26 G. M. Sheldrick, *Acta Crystallogr. Sect. C Struct. Chem.*, 2015, **71**, 3–8.

27 L. J. Barbour, *J. Supramol. Chem.*, 2001, **1**, 189–191.

28 O. V. Dolomanov, L. J. Bourhis, R. J. Gildea, J. A. K. Howard and H. Puschmann, *J. Appl. Crystallogr.*, 2009, **42**, 339–341.

29 Y. Shao, Z. Gan, E. Epifanovsky, A. T. B. Gilbert, M. Wormit, J. Kussmann, A. W. Lange, A. Behn, J. Deng, X. Feng, D. Ghosh, M. Goldey, P. R. Horn, L. D. Jacobson, I. Kaliman, R. Z. Khaliullin, T. Kuš, A. Landau, J. Liu, E. I. Proynov, Y. M. Rhee, R. M. Richard, M. A. Rohrdanz, R. P. Steele, E. J. Sundstrom, H. L. Woodcock, P. M. Zimmerman, D. Zuev, B. Albrecht, E. Alguire, B. Austin, G. J. O. Beran, Y. A. Bernard, E. Berquist, K. Brandhorst, K. B. Bravaya, S. T. Brown, D. Casanova, C. M. Chang, Y. Chen, S. H. Chien, K. D. Closser, D. L. Crittenden, M. Diedenhofen, R. A. Distasio, H. Do, A. D. Dutoi, R. G. Edgar, S. Fatehi, L. Fusti-Molnar, A. Ghysels, A. Golubeva-Zadorozhnaya, J. Gomes, M. W. D. Hanson-Heine, P. H. P. Harbach, A. W. Hauser, E. G. Hohenstein, Z. C. Holden, T. C. Jagau, H. Ji, B. Kaduk, K. Khistyaev, J. Kim, J. Kim, R. A. King, P. Klunzinger, D. Kosenkov, T. Kowalczyk, C. M. Krauter, K. U. Lao, A. D. Laurent, K. V. Lawler, S. V. Levchenko, C. Y. Lin, F. Liu, E. Livshits, R. C. Lochan, A. Luenser, P. Manohar, S. F. Manzer, S. P. Mao, N. Mardirossian, A. V. Marenich, S. A. Maurer, N. J. Mayhall, E. Neuscamman, C. M. Oana, R. Olivares-Amaya, D. P. Oneill, J. A. Parkhill, T. M. Perrine, R. Peverati, A. Prociuk, D. R. Rehn, E. Rosta, N. J. Russ, S. M. Sharada, S. Sharma, D. W. Small, A. Sodt, T. Stein, D. Stück, Y. C. Su, A. J. W. Thom, T. Tsuchimochi, V. Vanovschi, L. Vogt, O. Vydrov, T. Wang, M. A. Watson, J. Wenzel, A. White, C. F. Williams, J. Yang, S. Yeganeh, S. R. Yost, Z. Q. You, I. Y. Zhang, X. Zhang, Y. Zhao, B. R. Brooks, G. K. L. Chan, D. M. Chipman, C. J. Cramer, W. A. Goddard, M. S. Gordon, W. J. Hehre, A. Klamt, H. F. Schaefer, M. W. Schmidt, C. D. Sherrill, D. G. Truhlar, A. Warshel, X. Xu, A. Aspuru-Guzik, R. Baer, A. T. Bell, N. A. Besley, J. Da Chai, A. Dreuw, B. D. Dunietz, T. R. Furlani, S. R. Gwaltney, C. P. Hsu, Y. Jung, J. Kong, D. S. Lambrecht, W. Liang, C. Ochsenfeld, V. A. Rassolov, L. V. Slipchenko, J. E. Subotnik, T. Van Voorhis, J. M. Herbert, A. I. Krylov, P. M. W. Gill and M. Head-Gordon, *Mol. Phys.*, 2015, **113**, 184–215.

30 Q. Wu and T. Van Voorhis, *Phys. Rev. A - At. Mol. Opt. Phys.*, 2005, **72**, 7–10.

31 Q. Wu and T. Van Voorhis, *J. Chem. Phys.*, 2006, **125**, 164105.

32 Q. Wu, C. L. Cheng and T. Van Voorhis, *J. Chem. Phys.*, 2007, **127**, 164119.

33 J. Da Chai and M. Head-Gordon, *Phys. Chem. Chem. Phys.*, 2008, **10**, 6615–6620.

34 T. Brixner, R. Hildner, J. Köhler, C. Lambert and F. Würthner, *Adv. Energy Mater.*, 2017, **7**, 1–33.

35 N. J. Hestand and F. C. Spano, *Chem. Rev.*, 2018, **118**, 7069–7163.

36 S. K. Chakraborty, *Geofis. Pura Appl.*, 1956, **33**, 17-22.

37 R. Casier and J. Duhamel, *Macromolecules*, 2018, **51**, 3450–3457.

38 A. Gładysiak, T. N. Nguyen, R. Bounds, A. Zacharia, G. Itskos, J. A. Reimer and K. C. Stylianou, *Chem. Sci.*, 2019, **10**, 6140–6148.

39 J. H. Qin, Y. D. Huang, Y. Zhao, X. G. Yang, F. F. Li, C. Wang and L. F. Ma, *Inorg. Chem.*, 2019, **58**, 15013–15016.

40 A. Nakajima, *Bull. Chem. Soc. Jpn.*, 1973, 46, 2602–2604.

41 A. Sharma, D. Kim, J. H. Park, S. Rakshit, J. Seong, G. H. Jeong, O. H. Kwon and M. S. Lah, *Commun. Chem.*, 2019, **2**, 39.

42 F. C. Spano and C. Silva, *Annu. Rev. Phys. Chem.*, 2014, **65**, 477–500.

43 J. Hoche, H. C. Schmitt, A. Humeniuk, I. Fischer, R. Mitrić and M. I. S. Röhr, *Phys. Chem. Chem. Phys.*, 2017, **19**, 25002–25015.

44 P. Deria, J. Yu, T. Smith and R. P. Balaraman, *J. Am. Chem. Soc.*, 2017, **139**, 5973–5983.

45 R. D. Pensack, R. J. Ashmore, A. L. Paoletta and G. D. Scholes, *J. Phys. Chem. C*, 2018, **122**, 21004–21017.

46 J. B. Birks and L. G. Christophorou, *Spectrochim. Acta*, 1963, **19**, 401–410.

47 D. Sheberla, L. Sun, M. A. Blood-Forsythe, S. Er, C. R. Wade, C. K. Brozek, A. Aspuru-Guzik and M. Dincă, *J. Am. Chem. Soc.*, 2014, **136**, 8859–8862.

48 S. Patwardhan and G. C. Schatz, *J. Phys. Chem. C*, 2015, **119**, 24238–24247.

49 L. Sun, S. S. Park, D. Sheberla and M. Dincă, *J. Am. Chem. Soc.*, 2016, **138**, 14772–14782.

50 R. A. Marcus, *Annu. Rev. Phys. Chem.*, 1964, **15**, 155-196.

51 H. Kuroda, T. Amano, I. Ikemoto and H. Akamatu, *J. Am. Chem. Soc.*, 1967, **89**, 6056–6063.

52 W. P. Lustig, Z. Shen, S. J. Teat, N. Javed, E. Velasco, D. M. O'Carroll and J. Li, *Chem. Sci.*, 2020, **11**, 1814–1824.

53 C. Hou and H. Yu, *J. Mater. Chem. C*, 2020, **8**, 4169–4180.

54 J. Lu, W. Feng, G. Mei, J. Sun, C. Yan, D. Zhang, K. Lin, D. Wu, K. Wang and Z. Wei, *Adv. Sci.*, , DOI:10.1002/advs.202000689.

55 Y. K. Seo, J. W. Han, K. T. Lim, Y. H. Kim, C. W. Joo, J. Lee, N. S. Cho, S. Yu, M. H. Kang, C. Yun and B. H. Choi, *Org. Electron.*, 2017, **42**, 348–354.